Probing *n*-spin correlations in optical lattices

Chuanwei Zhang, V. W. Scarola, and S. Das Sarma

Condensed Matter Theory Center, Department of Physics, University of Maryland, College Park, Maryland 20742, USA

We propose a technique to measure multispin correlation functions of arbitrary range as determined by the ground states of spinful cold atoms in optical lattices. We show that an observation of the atomic version of the Stokes parameters, using focused lasers and microwave pulsing, can be related to *n*-spin correlators. We discuss the possibility of detecting not only ground state static spin correlations, but also time-dependent spin-wave dynamics as a demonstrative example using our proposed technique.

I. INTRODUCTION

The advent of optical lattice confinement of ultracold atomic gases [1–4] opens the possibility of observing a vast array of phenomena in quantum condensed systems [5]. In particular, optical lattice systems may turn out to be the ideal tools for the analog simulation of various strongly correlated interacting lattice models (e.g., Hubbard model [2,3], Kitaev model [6]) studied in solid state physics. The great advantage of optical lattices as analog simulators of strongly correlated Hamiltonians lies in the ability of optical lattices to accurately implement lattice models without impurities, defects, lattice phonons, and other complications which can obscure the observation of quantum degenerate phenomena in the solid state.

In this context optical lattices can support a variety of interacting spin models which to date have been only approximately or indirectly observed in nature or remain as rather deep but unobserved mathematical constructs. Three exciting possibilities are currently the subject of active study [5]. The first (and the most direct) envisions simulation of conventional condensed matter spin-lattice models in optical lattices. Quantum magnetism arising from strong correlation leads to many-body spin ground states that can be characterized by spin-order parameters. Spin order can, in some cases, show long-range behavior arising from spontaneous symmetry breaking, e.g., ferromagnetism and antiferromagnetism. Such long-range spin-ordering phenomena are reasonably well understood in most cases. Recent work also relates conventional spin-order parameters to entanglement measures which yield scaling behavior near quantum phase transitions [7,8]. The second possibility, simulation of topological spin states, arises from the surprising fact that optical lattices can also (at least in principle) host more complicated spin models previously thought to be academic. The ground states of these models do not fall within the conventional Landau paradigm, i.e., there is no spontaneously broken symmetry, but show topological ordering and, as a result, display nontrivial short-range behavior in spin correlation functions. Examples include the chiral spin-liquid model [9] and the Kitaev model [6,10–12]. Finally, optical lattices are also particularly well suited to realize coherent and collective spin dynamics because dissipation can be kept to suitably low levels [13].

While optical lattices offer the possibility of realizing all three of the above examples one glaring question remains.

Once a suitable spin Hamiltonian is realized, how do we observe the vast array of predicted phenomena in spin-optical lattices? To date, time-of-flight measurements have proven to yield detailed information related to two types of important correlation functions of many-body ground states of particles trapped in optical lattices. The first, a first-order correlation function (the momentum distribution), indicates ordering in one-point correlation functions [14]. The second is a second-order correlation function (the noise distribution) which indicates ordering in two-point density-density correlators [15–18]. The former can, for example, detect long-range phase coherence while, as we will see below, the latter is best suited to probe long-range order in two-point correlation functions, e.g., the lattice spin-spin correlation function. We note that recent proposals suggest that time-of-flight imaging can in principle be used to extract other correlation functions [19,20].

In this paper we propose a technique to observe equal time *n*-spin correlation functions characterizing *both* long- and short-range spin ordering useful in studying all three classes of spin-lattice phenomena mentioned above. Our proposal utilizes realistic experimental techniques involving focused lasers, microwave pulsing, and fluorescence detection to effectively measure a general *n*-spin correlation function defined by

$$\xi\{\alpha_{j_k}, k = 1, \ldots, n\} \equiv \langle\Psi|\prod_{k=1}^{n} \sigma_{j_k}^{\alpha_{j_k}}|\Psi\rangle, \qquad (1)$$

where Ψ is the many-body wave function of the atomic ensemble, $\{j_k\}$ is a set of sites, and $\sigma_{j_k}^{\alpha_{j_k}}$ ($\alpha_{j_k}=0,1,2,3$) are Pauli spin operators at sites j_k with the notation $\sigma^0=I$, $\sigma^1=\sigma^x$, $\sigma^2=\sigma^y$, and $\sigma^3=\sigma^z$. Examples of order detectable with one-, two-, and three-spin correlation functions are magnetization ($\langle\sigma_j^z\rangle=1$), antiferromagnetic order [$\langle\sigma_j^z\sigma_{j'}^z\rangle=(-1)^{j-j'}$], and chiral spin-liquid order [$\langle\sigma_j\cdot(\sigma_{j'}\times\sigma_{j''})\rangle=1$], to name a few.

In general our proposed technique can be used to experimentally characterize a broad class of spin-lattice models of the form

$$H(J;A) = J(t)\sum_{\{j_k\}}\left(A_{\{j_k\}}\prod_{k=1}^{M}\sigma_{j_k}^{\alpha_{j_k}}\right), \qquad (2)$$

where *J* has dimensions of energy and can vary adiabatically as a function of time, *t*, while the dimensionless parameters

$A_{\{j_k\}}$ are kept fixed. For example, $M=2$ represents the usual two-body Heisenberg model. Several proposals now exist for simulating two-body Heisenberg models [5,10]. In the following we, as an example, consider optical lattice implementations of the Heisenberg XXZ model,

$$H_{XXZ}(J;\Delta) = J\left(\sum_{\langle j,j' \rangle} (\sigma_j^x \sigma_{j'}^x + \sigma_j^y \sigma_{j'}^y) + \Delta \sigma_j^z \sigma_{j'}^z \right), \quad (3)$$

where $\langle j,j' \rangle$ denotes nearest neighbors and Δ and J are model parameters that can be adjusted by, for example, varying the intensity of lattice laser beams [10].

The paper is organized as follows: in Sec. II we show that, in practice, short-range spin correlations are difficult to detect in noise correlation measurements. Section III lays out a general procedure for detecting n-spin correlations with local probes. An experimental scheme for realizing such a procedure is proposed and a quantitative feasibility analysis is presented. Section IV is devoted to an investigation of the time dependence of correlation functions using the technique. In particular, we show how the technique can be used to engineer and probe spin-wave dynamics. We conclude in Sec. V.

II. LOCAL CORRELATIONS IN TIME OF FLIGHT

We first discuss the measurement of spin-spin correlation functions by analyzing spatial noise correlations (two-point density-density correlations), i.e., $[\langle n(\vec{r})n(\vec{r}') \rangle - \langle n(\vec{r}) \rangle \times \langle n(\vec{r}') \rangle]/\langle n(\vec{r}) \rangle \langle n(\vec{r}') \rangle$ in time-of-flight images from atoms confined to an optical lattice modeled by the XXZ Hamiltonian. The ground states of this and a variety of spin models can be characterized by the spin-spin correlation function between different sites. For instance, the spin-spin correlation function in a one-dimensional XXZ spin chain (with $J>0$), shows power-law decay

$$\langle \sigma_j^z \sigma_{j'}^z \rangle \sim (-1)^{j-j'}/|j-j'|^\eta \quad (4)$$

in the critical regime $(-1 < \Delta \leq 1)$, where $\eta = 1/(1 - \frac{1}{\pi}\cos^{-1}\Delta)$. In principle this correlation function can be probed by spatial noise correlation in time of flight.

We argue that, in practice, short-range correlations (e.g., $\eta > 1$ in the XXZ model) are difficult to detect in time-of-flight noise correlation measurements. To see this note that the noise correlation signal is proportional to [15]

$$G[Q(r-r')] = \sum_{j,j'} e^{iQ(j'-j)a} \langle \sigma_j^z \sigma_{j'}^z \rangle, \quad (5)$$

where Q is the lattice wave vector which gets mapped into coordinates r and r' in time of flight on the detection screen, and a is the lattice spacing. Including normalization the noise correlation signal is proportional to N^{-1} for systems with long-range order (e.g., antiferromagnetic order giving $\eta=0$ in the above XXZ model) but shows a much weaker scaling for short-range correlations. In fact the *ratio* between correlators in a ground state with $\eta > 1$ (short-range power-law order) and $\eta=0$ (long-range antiferromagnetic order) scales as N^{-1} making the state with power-law correlations rela-
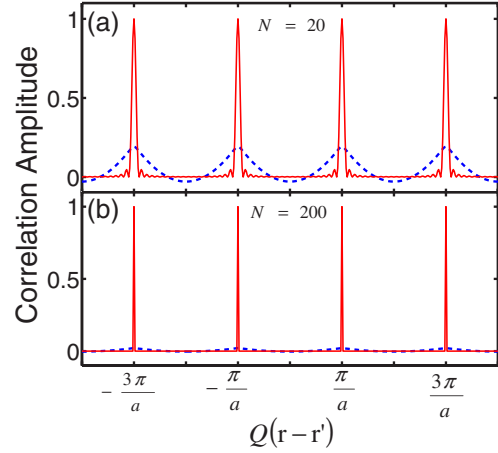

FIG. 1. (Color online) Noise correlation plotted as a function of wave vector of the one-dimensional XXZ model. The solid (dashed) line corresponds to a ground state with $\eta=0$, long-range ($\eta=2$, short-range) spin correlator. The amplitudes are normalized by the maximum for antiferromagnetic order ($\eta=0$). The number of atoms in panels (a) and (b) are $N=20$ and $N=200$, respectively.

tively difficult to detect in large systems. To illustrate this we compare the calculated noise correlation amplitude, G, in Fig. 1 for two cases $\eta=0$ (solid line) and $\eta=2$ (dashed line) with $N=20$ [Fig. 1(a)] and $N=200$ [Fig. 1(b)] for the 1D XXZ model. We see that the correlation amplitude for short-range (power-law) order is extremely small in comparison to long-range antiferromagnetic order for large N.

The small correlation signal originates from the fact that the noise correlation method is in practice a conditional probability measuring collective properties of the whole system, while short-range spin correlations describe local properties and are therefore best detected via local operations. In the following we propose a local probe technique to measure local correlations thus providing an experimental scheme which compliments the time-of-flight–noise correlation technique, best suited for detecting long-range order.

III. DETECTING n-SPIN CORRELATION WITH LOCAL PROBES

A. General procedure

We find that general n-spin correlators, $\xi\{\alpha_{j_k}, k=1,\ldots,n\}$, can be related to the Stokes parameters broadly defined in terms of the local reduced density matrix $\rho = \text{Tr}_{\{j_k, k=1,\ldots,n\}} |\Psi\rangle\langle\Psi|$ on sites $\{j_k, k=1,\ldots,n\}$, where the trace is taken on all sites except the set $\{j_k\}$. The Stokes parameters [21] for the density matrix ρ are $S_{\alpha_{j_1}\cdots\alpha_{j_n}} = \text{Tr}(\rho \Pi_{k=1}^n \sigma_{j_k}^{\alpha_{j_k}})$ leading to the decomposition

$$\rho = 2^{-n} \sum_{\alpha_{j_1},\cdots,\alpha_{j_n}=0}^{3} \left(S_{\alpha_{j_1}\cdots\alpha_{j_n}} \prod_{k=1}^n \sigma_{j_k}^{\alpha_{j_k}} \right). \quad (6)$$

Using the theory of quantum state tomography [21], we find the n-spin correlators

$$\xi\{\alpha_{j_k}, k=1,\ldots,n\} = \prod_{k=1}^{n} (P\{|\phi_{\alpha_{j_k}}\rangle\} \pm P\{|\phi_{\alpha_{j_k}}^{\perp}\rangle\}), \qquad (7)$$

where the plus (minus) sign indicates a 0 (nonzero) index and $\{|\phi_{\alpha_{j_k}}\rangle, |\phi_{\alpha_{j_k}}^{\perp}\rangle\}$ denote the measurement basis for the atom at j_k. We define the measurement basis to be $|\phi_1\rangle = (|\downarrow\rangle + |\uparrow\rangle)/\sqrt{2}$, $|\phi_1^{\perp}\rangle = (|\downarrow\rangle - |\uparrow\rangle)/\sqrt{2}$, $|\phi_2\rangle = (|\downarrow\rangle + i|\uparrow\rangle)/\sqrt{2}$, $|\phi_2^{\perp}\rangle = (|\downarrow\rangle - i|\uparrow\rangle)/\sqrt{2}$, $|\phi_3\rangle = |\downarrow\rangle$, $|\phi_3^{\perp}\rangle = |\uparrow\rangle$. Finally, $P\{|\phi_{\alpha_{j_k}}\rangle\}$ is the probability of finding an atom in the state $|\phi_{\alpha_{j_k}}\rangle$.

The expansion of the product defining ξ then yields a quantity central to our proposal,

$$\xi\{\alpha_{j_k}, k=1,\ldots,n\} = \sum_{l=1}^{n} (-1)^l P_l, \qquad (8)$$

where P_l is the probability of finding l sites in the states $|\phi_{j_k}^{\perp}\rangle$ and $n-l$ sites in $|\phi_{j_k}\rangle$. Equation (8) shows that the n-spin correlation function can be written in terms of experimental observables. We can now write a specific example of the two-spin correlation function (discussed in the preceding section) in terms of observables: $\xi\{3,3\} = P_{|\downarrow\rangle_{j_1}|\downarrow\rangle_{j_2}} + P_{|\uparrow\rangle_{j_1}|\uparrow\rangle_{j_2}} - (P_{|\downarrow\rangle_{j_1}|\uparrow\rangle_{j_2}} + P_{|\uparrow\rangle_{j_1}|\downarrow\rangle_{j_2}})$. In the following subsection we discuss a specific experimental procedure designed to extract precisely this quantity using local probes of cold atoms confined to optical lattices.

B. Proposed experimental realization

We now describe and critically analyze an experimental procedure designed to find the probabilities, P_l, from which we can determine the spin-correlation function $\xi\{\alpha_{j_k}, k=1,\ldots,n\}$ through Eq. (8). To illustrate our technique we consider a specific experimental system: ^{87}Rb atoms confined on a single two-dimensional (xy plane) optical lattice with two hyperfine ground states $|\downarrow\rangle \equiv |F=1, m_F=-1\rangle$ and $|\uparrow\rangle \equiv |F=2, m_F=-2\rangle$ chosen as the spin of each atom. Here the atomic dynamics in the z direction are frozen out by high frequency optical traps [22]. However, the scheme can be directly applied to three-dimensional optical lattices by using one additional focused laser which propagates along the xy plane and plays the same role as the focused laser (propagating along the z axis) discussed in the following step (II).

In the Mott insulator regime with one atom per lattice site spin Hamiltonians, defined in Eq. (2), may be implemented using spin-dependent lattice potentials in the superexchange limit [10]. The spin coupling $J(t)$, i.e., the overall prefactor in Eq. (2), can be controlled by varying the lattice depth. Our proposed experimental procedure will build on such spin systems, although it can be generalized to other implementations where H is generated by other means. In the spin systems, the ground states are strongly correlated many-body spin states and their properties can be characterized by the spin correlations between atoms at different lattice sites.

Step (I). We start with a many-body spin state Φ_0 and turn off the spin-spin interactions generated by superexchange between lattice sites. We achieve this by ramping up the spin-dependent lattice depth to $\sim 50 E_R$ adiabatically with respect
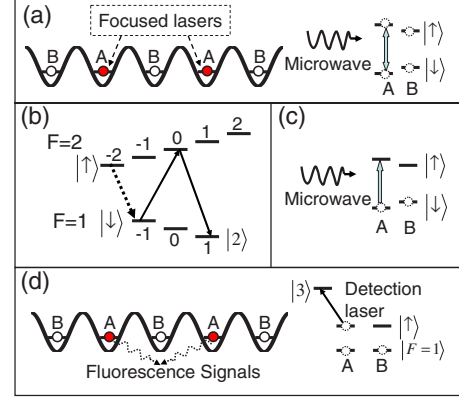

FIG. 2. (Color online) Schematic plot of the experimental procedure used to measure n-spin correlation functions. A indicates one of the target atoms. B indicates all other atoms. (a) Target atoms A are transferred to a suitable measurement basis using a combination of focused lasers and microwave pulses [see step (II)]. (b) Atoms at state $|\downarrow\rangle$ are transferred to state $|2\rangle$ by two microwave π pulses, then atoms at state $|\uparrow\rangle$ are transferred to state $|\downarrow\rangle$ by another microwave π pulse [see step (III)]. (c) Target atoms A are transferred back to state $|\uparrow\rangle$ from $|\downarrow\rangle$ [see step (IV)]. (d) A detection laser is applied to detect the probability of finding target atoms at $|\uparrow\rangle$ [see step (IV)].

to the band splitting, where $E_R = h^2/2m\lambda^2$ is the photon recoil energy and λ is the wavelength of the optical lattice. The ramp up time for each lattice is chosen properly so that only the overall energy scale $J(t)$ in the spin Hamiltonian (2) is modified, which preserves the highly correlated spin state Φ_0. In the deep lattice, the time scale for the spin-spin interactions ($\sim \hbar/J > 10 s$) becomes much longer than the time (~ 1 ms) taken to perform the spin-correlation measurement. The spin-spin interactions play no role in the measurement process and the following detection steps are quickly performed on this "frozen" many-body spin state Φ_0.

Step (II). In this step, we selectively transfer target atoms A at site(s) j_k (chosen *a priori*) to a suitable measurement basis $\{|\phi_{j_k}\rangle, |\phi_{j_k}^{\perp}\rangle\}$ from initial states $\{|\downarrow\rangle_{j_k}, |\uparrow\rangle_{j_k}\}$, without affecting nontarget atoms B at other sites [Fig. 2(a)]. Selective manipulation of quantum states of single atoms in optical lattices is currently an outstanding challenge for investigating physics in an optical lattice, because spatial periods of typical optical lattices are shorter than the optical resolution. In Ref. [23], a scheme for single atom manipulation using microwave pulses and focused lasers is proposed and analyzed in detail. Here we apply the scheme to selectively transfer atoms between different measurement bases.

To manipulate a target atom A, we adiabatically turn on a focused laser that propagates along the $\hat{z}$ axis having the maximal intensity located at A. The spatially varying laser intensity $I(\mathbf{r})$ induces position-dependent energy shifts

$$\Delta E_i(\mathbf{r}) = \beta_i I(\mathbf{r}) \qquad (9)$$

for two spin states $|\downarrow\rangle$ and $|\uparrow\rangle$, where the parameter β_i for state $|i\rangle$ ($i=\downarrow$ or $\uparrow$) is determined by the focused laser parameters. Different polarizations and detunings of the focused laser lead to different β_i and thus yield different shifts of the

hyperfine splittings $|\Delta E(\mathbf{r})| = |\Delta E_{\uparrow}(\mathbf{r}) - \Delta E_{\downarrow}(\mathbf{r})|$ between two spin states. We choose a σ^+-polarized laser that drives the $5S \rightarrow 6P$ transition to obtain a small diffraction limit. The wavelength $\lambda_f \approx 421$ nm (corresponding to a detuning $\Delta_0 = -2\pi \times 1209$ GHz from the $6\,^2P_{3/2}^2$ state) is optimized to obtain the maximal ratio between energy splittings of two spin states and the spontaneous scattering rate [23].

Because of the inhomogeneity of the focused laser intensity $I(\mathbf{r})$, $|\Delta E(\mathbf{r})|$ reaches a maximum at the target atom A and decreases dramatically at neighboring sites. Therefore the degeneracy of hyperfine splittings between different atoms is lifted. By adjusting the focused laser intensity, the differences of the energy shifts $\delta = |\Delta E(0)| - |\Delta E(\lambda/2)|$ between target atom A and nontarget neighboring atom B can be varied and calculated through Eq. (9). Here we choose $\delta = 74E_R$ because it balances the speed and fidelity of single spin manipulation, leading to less spontaneously scattered photons from the target atoms in the spin-dependent focused lasers. To avoid excitations of atoms to higher bands of the optical lattice, the rise speed of the focused laser intensity should satisfy the adiabatic condition. We use the adiabatic condition to estimate the ramp up time of the focused laser to be 35 μs to give a 10^{-4} probability for excitation to higher bands.

We then change the measurement basis by applying a microwave $\pi/2$ pulse that drives a suitable rotation to target atoms A [Fig. 2(a)]. The microwave is resonant with the hyperfine splitting between two spin states of the target atoms A, but has a detuning larger than δ for nontarget atoms B. Consider a pulse with Rabi frequency

$$\Omega(t) = \Omega_0 \exp(-\omega_0^2 t^2) \ (-t_f \le t \le t_f)$$

and parameters $\omega_0 = 14.8E_R/\hbar$, $\Omega_0 = 13.1E_R/\hbar$, and $t_f = 5/\omega_0$. The pulse transfers the measurement basis of the target atoms A in 16.9 μs, while the change in the quantum state of nontarget atoms is found to be below 3×10^{-4} by numerically integrating the Rabi equation that describes the coupling between two spin states by the microwave pulse. The focused lasers are adiabatically turned off after the microwave pulse. During the step (II), the probability for spontaneous scattering of one photon from target atoms inside the focused laser can be roughly estimated as $P \approx \int_{\tau_i}^{\tau_f} \frac{\Gamma}{\hbar \vartheta} V(t) dt \sim 2 \times 10^{-4}$, where τ_i and τ_f represent the times when the focused laser is turned on and off, Γ is the decay rate of $6P$ state, ϑ is the detuning, and $V(t)$ is the potential depth of the focused laser.

The distance between any two target atoms can be as short as a lattice spacing. This is because the basis transfer processes for different target atoms are preformed sequentially in time, i.e., the process for an atom at site j_2 starts after the process for an atom at site j_1 is accomplished. In the special case that sites j_1 and j_2 are spatially well separated and the final basis $\{|\phi_{j_k}\rangle, |\phi_{j_k}^{\perp}\rangle\}$ at two sites are the same, the transfer process can be done simultaneously for two sites with one microwave pulse.

Step (III). In this step, we transfer all atoms to the $|F=1\rangle$ hyperfine level [Fig. 2(b)] to avoid stray signal in the detection step (IV). We apply two π microwave pulses to
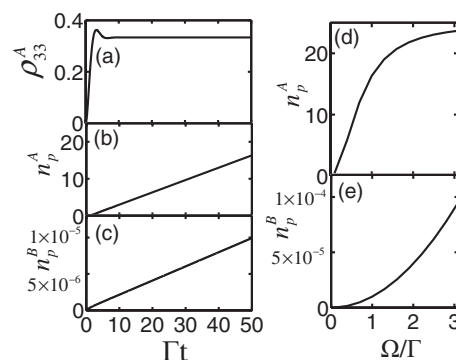

FIG. 3. (a) Time evolution of the probability for the target atoms A to be in the excited state $|3\rangle$. (b) The number of scattering photons n_p^A versus time for atoms A at state $|\uparrow\rangle$. (c) The number of scattering photons n_p^B versus time for atoms (A or B) at states $|\downarrow\rangle$ and $|2\rangle$. (d) The number of scattering photons n_p^A versus the Rabi frequency of the resonant laser for atoms A at state $|\uparrow\rangle$. (e) The number of scattering photons n_p^B versus the Rabi frequency of the resonant laser for atoms (A or B) at states $|\downarrow\rangle$ and $|2\rangle$. The time period for (d) and (e) is $50/\Gamma$.

transfer all atoms at $|\downarrow\rangle$ first to $|F=2, m_F=0\rangle$ then to $|2\rangle \equiv |F=1, m_F=1\rangle$. Another π microwave pulse is then applied to transfer all atoms at $|\uparrow\rangle$ to $|\downarrow\rangle$. The π microwave pulse can be implemented within 12.5 μs for a microwave Rabi frequency $\Omega = 2\pi \times 40$ kHz.

Step (IV). We transfer target atoms A at j_k from $|\downarrow\rangle$ back to $|\uparrow\rangle$ with the assistance of the focused lasers and microwave pulses [Fig. 2(c)], using the same atom manipulation procedure as that described in step (II). We then apply a detection laser resonant with

$$|\uparrow\rangle \rightarrow |3\rangle \equiv |5\,^2P_{3/2}:F=3, m=-3\rangle$$

to detect the probability of finding all target atoms at $|\uparrow\rangle$ [corresponding to the basis state $|\phi_{j_k}^{\perp}\rangle$ because we transferred atoms to the measurement basis in step (II)] [Fig. 2(d)]. The beam size of the detection laser should be large enough so that target atoms at different sites $\{j_k\}$ experience the same laser intensity, and scatter the same number of photons if they are in the $|\uparrow\rangle$ state. The fluorescence signal (the number of scattered photons) is from one of the $n+1$ quantized levels, where the lth level $(l=0, \ldots, n)$ corresponds to states with l sites of target atoms on state $|\uparrow\rangle$ $(|\phi_{j_k}^{\perp}\rangle)$. By repeating the whole process many times, we obtain the probability distribution P_l, and thus the spin correlation function $\xi\{\alpha_{j_k}, k=1, \ldots, n\}$ via Eq. (8).

The scattering photons of the fluorescence signals come mostly from the target atoms A at state $|\uparrow\rangle$ (Fig. 3). Signal from atoms at any $|F=1\rangle$ state is suppressed because of the large hyperfine splitting ($\nu \approx 2\pi \times 6.8$ GHz) between $|F=1\rangle$ and $|F=2\rangle$ states. Atoms B do not contribute to the fluorescence signal because they are already transferred to the $|F=1\rangle$ state in step (III). The dynamics of photon scattering is described by the optical Bloch equation [24],

$$\frac{d}{dt}\rho_{33} = -\Gamma\rho_{33} + \frac{i}{2}\Omega(\rho_{13} - \rho_{31}),$$

$$\frac{d}{dt}\rho_{13} = -\left(\frac{\Gamma}{2}+i\nu_0\right)\rho_{13} + \frac{i}{2}\Omega(2\rho_{33}-1),$$

$$\frac{d}{dt}\rho_{31} = -\left(\frac{\Gamma}{2}-i\nu_0\right)\rho_{31} - \frac{i}{2}\Omega(2\rho_{33}-1), \qquad (10)$$

where $\rho_{33}(t) = |c_3(t)|^2$ is the probability for the atom to be in the excited state $|3\rangle$, $|1\rangle$ represents state $|\uparrow\rangle$ for target atom A at state $|\uparrow\rangle$ and $|F=1\rangle$ for other cases, $\rho_{13}(t) = c_1(t)c_3^*(t)e^{i\nu_0 t}$, $\rho_{31}(t) = \rho_{13}^*(t)$. The detuning of the laser ν_0 is zero for target atoms A at state $|\uparrow\rangle$ and $\sim\nu$ for all nontarget atoms B and part of the target atoms A at hyperfine state $|2\rangle$. $\Gamma = 2\pi \times 6.07$ MHz is the decay rate of the excited state $|3\rangle$, Ω is the Rabi frequency of the resonant laser that is related to the on-resonance saturation parameter by $s_0 = 2|\Omega|^2/\Gamma^2$.

We numerically integrate the optical Bloch equation and calculate the number of scattering photons

$$n_p(t) = \Gamma \int_0^t \rho_{33}(t')dt' \qquad (11)$$

for both target and nontarget atoms. In Fig. 3(a), we plot the probability ρ_{33}^A for target atoms A at state $|3\rangle$ with respect to time. We see ρ_{33}^A increases initially and reaches the saturation value $s_0/2(1+s_0)$. The number of scattering photons reaches 20 in a short period, 1.3 μs for atoms A at $|\uparrow\rangle$ [Fig. 3(b)], but it is only 10^{-5} for nontarget atoms B and target atoms A at state $|2\rangle$ [Fig. 3(c)]. Therefore the impact of the resonant laser on the nontarget atoms B can be neglected. In Figs. 3(d) and 3(e), we see that for a wide range of Rabi frequencies (laser intensities), the scattering photon number for the nontarget atoms B is suppressed to undetectable levels, below 10^{-4}.

Unlike the noise correlation method, the accuracy of our detection scheme does not scale with the number of total atoms N, but is determined only by manipulation errors in the above steps. We roughly estimate that n-spin correlations can be probed with a cumulative error $<n\times 10^{-2}$, which is sufficient to measure both long- and short-range spin-correlation functions. Our estimate takes into account possible experimental errors in all four steps, and the fact that the same experimental procedure is repeated many times to determine the probability P_l. The total failure probability of the four-step detection process is $p(n)\sim n\times 10^{-3}$ for n target atoms to give an incorrect measurement of the target atom quantum state for determining the quantity P_l. Assuming that the experimental procedure is repeated ν times, the total probability for obtaining one incorrect measurement result is about $\nu p(n)$. Since one incorrect measurement result leads to an error $\sim 1/\nu$ in P_l, the expectation for the error is $\nu p(n) \times 1/\nu = p(n)$, which should be chosen to be $1/\nu$ to minimize the total error. In addition, the uncertainty in measurements of probability P_l itself in repeated experiments is also about $1/\nu$. Taking into account all of these errors, we find that n-spin correlations can be probed with an error that scales as $Cp(n)$, where $C\sim 3$ in our rough estimate. As a conservative

estimate, we take $C=10$ to give an overall error in measuring n-spin correlation function $\xi\{\alpha_{j_k}, k=1,\ldots,n\}$ to be less than $10p(n)\sim n\times 10^{-2}$.

We note that the scheme requires repeated production of nearly the same condensate and repeated measurements, two standard techniques which have been realized in many experiments. We have proposed a powerful technique for investigating strongly correlated spin models in optical lattices and now consider one of several possible applications.

IV. SPIN-WAVE DYNAMICS

Our technique can be used to investigate time dependence of correlation functions. In the following, we show how our scheme can be used to engineer and probe spin-wave dynamics in a straightforward example, the Heisenberg XX model realized in optical lattices with a slightly different implementation scheme than the one discussed in the preceding section. Consider a Mott insulator state with one boson per lattice site prepared in the state $|0\rangle \equiv |F=1, m_F=-1\rangle$ in a three-dimensional optical lattice. By varying the trap parameters or with a Feshbach resonance, the interaction between atoms can be tuned to the hard-core limit. With large optical lattice depths in the y and z directions, the system becomes a series of one-dimensional tubes with dynamics described by the Bose-Hubbard Hamiltonian,

$$H_s = -\chi(t)\sum_j (a_j^\dagger a_{j+1} + a_{j+1}^\dagger a_j). \qquad (12)$$

This Bose-Hubbard model can be solved exactly. It offers a testbed for spin-wave dynamics by mapping the Hamiltonian (12) onto the XX spin model, $H_{XXZ}(-2\chi; \Delta=0)$, with the Holstein-Primakoff transformation [25].

We now study the time-dependent behavior of the XX model using our proposed scheme. In the Heisenberg picture, the time evolution of the annihilation operator can be written as $a_j(t) = \sum_{j'} a_{j'}(0)i^{j'-j}J_{j'-j}(\alpha)$, where $J_{j'-j}(\alpha)$ is the Bessel function of the interaction parameter $\alpha(t) = 2\int_0^t \chi(t')dt'$. To observe spin-wave dynamics, we first flip the spin at one site from $\uparrow$ to $\downarrow$, which, in the bosonic degrees of freedom, corresponds to removing an atom at that site. Because of the spin-spin interactions, initial ferromagnetic order gives way to a reorientation of spins at neighboring sites which propagates along the spin chain in the form of spin waves. This corresponds to a time-dependent oscillation of atom number at each site. Therefore, spin-wave dynamics can be studied in one- and two-point spin-correlation functions by detecting the oscillation of the occupation probability at certain sites and the density-density correlator between different sites, respectively.

Single atom removal at specific sites can be accomplished with the assistance of focused lasers. With a combination of microwave radiation and two focused lasers (propagating along y and z directions, respectively), we can selectively transfer an atom at a certain site from the state $|0\rangle$ to the state $|4\rangle \equiv |F=2, m_F=-2\rangle$. A laser resonant with the transition $|4\rangle \to |3\rangle \equiv |5\,^2P_{3/2}: F=3, m=-3\rangle$ is then applied to remove an atom at that site. Following an analysis similar to the one

above, we see that the impact on other atoms can be neglected. To observe fast dynamics of spin-wave propagation, we may adiabatically ramp down the optical lattice depth (and therefore increase χ) from the initial depth $V_0 = 50 E_R$ to a final depth $13 E_R$, with a hold time, t_{hold}, to let the spin wave propagate. Finally, the lattice depth is adiabatically ramped back up to V_0 for measurement. The time dependence of the lattice depth in the ramping down process is chosen to be

$$V(t) = V_0 / (1 + 4\sqrt{2 P_{\text{exe}} V_0 / E_R} \, \omega_r t), \tag{13}$$

where P_{exe} is the probability of making an excitation to higher bands and $\omega_R = E_R / \hbar$. For $P_{\text{exe}} = 4 \times 10^{-4}$, we find the interaction parameter to be $\alpha(t_{\text{hold}}) = 0.0146 + 0.0228 \omega_R t_{\text{hold}}$, with the tunneling parameter

$$\chi(t) = (4/\sqrt{\pi}) E_R^{1/4} V^{3/4}(t) \exp[-2\sqrt{V(t)/E_R}]. \tag{14}$$

Two physical quantities that can be measured in experiments are the single atom occupation probability

$$D_j(\alpha) = \langle \varphi | a_j^\dagger a_j | \varphi \rangle = \sum_{l \neq \kappa} J_{l-j}^2(\alpha) \tag{15}$$

at the site j, and the density-density correlator

$$G_{jj'}(\alpha) = \langle \varphi | a_j^\dagger a_j a_{j'}^\dagger a_{j'} | \varphi \rangle = \sum_{l \neq \kappa, \gamma \neq \kappa} J_{l-j}^2(\alpha) J_{\gamma-j'}^2(\alpha)$$

$$- \sum_{l \neq \kappa} [J_{l-j}^2(\alpha) J_{l-j'}^2(\alpha)$$

$$+ J_{l-j}(\alpha) J_{\kappa-j}(\alpha) J_{\kappa-j'}(\alpha) J_{l-j'}(\alpha)] \tag{16}$$

between sites j and j', where φ is the initial wave function with one removed atom at site κ. The former is related to the local transverse magnetization through

$$\langle \varphi | s_j^z(\alpha) | \varphi \rangle = D_j(\alpha) - 1/2, \tag{17}$$

and the latter is related to the spin-spin correlator via

$$G_{jj'}(\alpha) = \langle \varphi | s_j^z(\alpha) s_{j'}^z(\alpha) | \varphi \rangle + [D_j(\alpha) + D_{j'}(\alpha)]/2 + 1/4. \tag{18}$$

In Fig. 4, we plot $D_j(\alpha)$ and $G_{jj'}(\alpha)$ with respect to the interaction parameters α (which scales linearly with holding time). Here the initial empty site at $j=0$ is located at the center of the spin lattice. We see different oscillation behavior at different sites. Initially, all sites are occupied except $j=0$, i.e., $D_{j \neq 0}(0) = 1$, $D_{j=0}(0) = 0$ [Fig. 4(a)]. The initial spin-spin correlation $G_{jj'}(0)$ between different sites is zero if either j or j' is zero, and one if both of them are nonzero [Fig. 4(b)]. As α increases, atoms start to tunnel between neighboring sites and the spin wave propagates along the one-dimensional optical lattice, which is clearly indicated by the
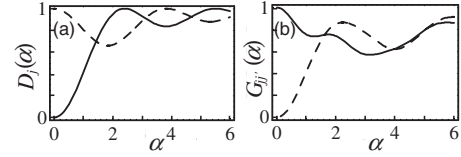

FIG. 4. Site occupation probability (a) and density-density correlation (b) with respect to scaled spin interaction parameter $\alpha \propto$ time for $N=30$ and $j=0$ [(a) solid line]; $j=1$ [(a) dashed line]; $j=0$, $j'=3$ [(b) dashed line]; and $j=2$, $j'=3$ [(b) solid line]. The site index j ranges from $-N$ to N.

increase (decrease) of the site occupation at $j=0$ ($j \neq 0$). In Fig. 4, the oscillation of $D_j(\alpha)$ and $G_{jj'}(\alpha)$ in a long time period and the decay of the oscillation amplitudes originate from the finite size of the spin lattice, which yields the reflection of the spin waves at the boundaries.

To probe the single site occupation probability $D_j(\alpha)$, we use two focused lasers and one microwave pulse to transfer the atom at site j to $|4\rangle$. A laser resonant with the transition $|4\rangle \rightarrow |3\rangle$ is again applied to detect the probability to have an atom at $|4\rangle$, which is exactly the occupation probability $D_j(\alpha)$. To detect $G_{jj'}(\alpha)$, we transfer atoms at both sites j and j' to the state $|4\rangle$ and use the same resonant laser to detect the joint probability for atoms at $|4\rangle$. The fluorescence signal has three levels, which correspond to both atoms $G_{jj'}(\alpha)$, one atom $D_j(t) + D_{j'}(t)$, and no atoms at state $|4\rangle$. A combination of these measurement results gives the spin-spin correlator $\langle \varphi | s_j^z(\alpha) s_{j'}^z(\alpha) | \varphi \rangle$.

V. CONCLUSION

We find that a relation between general spin-correlation functions and observable state occupation probabilities in optical lattices allows for quantitative measurements of a variety of spin correlators with the help of local probes, specifically focused lasers and microwave pulsing. Our proposal includes a realistic and practical quantitative analysis suggesting that n-spin correlations can be probed with an error $< n \times 10^{-2}$, which is sufficient to measure both long- and short-range spin-correlation functions. Our work establishes a practical and workable method for detecting n-spin correlations for cold atoms in one-, two- or three-dimensional optical lattices. Applications to a broad class of spin physics including topological phases of matter [6,12] realized in spin-optical lattices are also possible with our proposed technique.

[1] P. S. Jessen, C. Gerz, P. D. Lett, W. D. Phillips, S. L. Rolston, R. J. C. Spreeuw, and C. I. Westbrook, Phys. Rev. Lett. **69**, 49 (1992).

[2] D. Jaksch, C. Bruder, J. I. Cirac, C. W. Gardiner, and P. Zoller, Phys. Rev. Lett. **81**, 3108 (1998).

[3] M. Greiner, O. Mandel, T. Esslinger, T. W. Hänsch, and I. Bloch, Nature (London) **415**, 39 (2002).

[4] B. Paredes, A. Widera, V. Murg, O. Mandel, S. Foelling, I. Cirac, G. V. Shlyapnikov, T. W. Hänsch, and I. Bloch, Nature (London) **429**, 277 (2004).

[5] M. Lewenstein, A. Sanpera, V. Ahufinger, B. Damski, A. Sen De, and U. Sen, Adv. Phys. **56**, 243 (2007).

[6] A. Kitaev, Ann. Phys. **321**, 2 (2006).

[7] A. Osterloh, L. Amico, G. Falci, and R. Fazio, Nature (London) **416**, 608 (2002).

[8] T. Roscilde, P. Verrucchi, A. Fubini, S. Haas, and V. Tognetti, Phys. Rev. Lett. **93**, 167203 (2004); **94**, 147208 (2005).

[9] X. G. Wen, F. Wilczek, and A. Zee, Phys. Rev. B **39**, 11413 (1989).

[10] L.-M. Duan, E. Demler, and M. D. Lukin, Phys. Rev. Lett. **91**, 090402 (2003).

[11] A. Micheli, G. K. Brennen, and P. Zoller, Nature Phys. **2**, 341 (2006).

[12] C. Zhang, V. W. Scarola, S. Tewari, and S. Das Sarma, e-print arXiv:quant-ph/0609101.

[13] A. Widera, F. Gerbier, S. Folling, T. Gericke, O. Mandel, and I. Bloch, Phys. Rev. Lett. **95**, 190405 (2005); F. Gerbier, A. Widera, S. Folling, O. Mandel, and I. Bloch, Phys. Rev. A **73**, 041602(R) (2006).

[14] W. Ketterle, D. S. Durfee, and D. M. Stamper-Kurn, e-print arXiv:cond-mat/9904034.

[15] E. Altman, E. Demler, and M. D. Lukin, Phys. Rev. A **70**, 013603 (2004).

[16] M. Greiner, C. A. Regal, C. Ticknor, J. L. Bohn, and D. S. Jin, Phys. Rev. Lett. **92**, 150405 (2004).

[17] S. Foelling, F. Gerbier, A. Widera, O. Mandel, T. Gericke, and I. Bloch, Nature (London) **434**, 481 (2005).

[18] I. B. Spielman, W. D. Phillips, and J. V. Porto, Phys. Rev. Lett. **98**, 080404 (2007).

[19] L.-M. Duan, Phys. Rev. Lett. **96**, 103201 (2006).

[20] Q. Niu, I. Carusotto, and A. B. Kuklov, Phys. Rev. A **73**, 053604 (2006).

[21] J. B. Altepeter *et al.*, in *Quantum State Estimation*, edited by M. G. A. Paris and J. Rehacek (Springer, Berlin, 2004).

[22] T. P. Meyrath, F. Schreck, J. L. Hanssen, C.-S. Chuu, and M. G. Raizen, Phys. Rev. A **71**, 041604(R) (2005).

[23] C. Zhang, S. L. Rolston, and S. Das Sarma, Phys. Rev. A **74**, 042316 (2006).

[24] H. J. Metcalf and P. van der Straten, *Laser Cooling and Trapping* (Springer-Verlag, New York, 1999).

[25] A. Auerbach, *Interacting Electrons and Quantum Magnetism* (Springer-Verlag, New York, 1994).